Journal of Applied Geophysics 146 (2017) 16–26

Contents lists available at ScienceDirect

Journal of Applied Geophysics

journal homepage: www.elsevier.com/locate/jappgeo

# Electrical and seismic response of saline permafrost soil during freeze - Thaw transition

Yuxin Wu [a,*], Seiji Nakagawa [b], Timothy J. Kneafsey [b], Baptiste Dafflon [a], Susan Hubbard [a]

[a] Climate and Ecosystem Sciences Division, Lawrence Berkeley National Laboratory, Berkeley, CA 94720, USA
[b] Energy Geosciences Division, Lawrence Berkeley National Laboratory, Berkeley, CA 94720, USA

ARTICLE INFO

*Article history:*
Received 21 March 2017
Received in revised form 15 August 2017
Accepted 17 August 2017
Available online 30 August 2017

*Keywords:*
Saline permafrost
Electrical resistivity
Induced polarization
Seismic property
Freeze – thaw
Unfrozen water content

ABSTRACT

We conducted laboratory studies on the geophysical signals from Arctic saline permafrost soils to help understand the physical and mechanical processes during freeze-thaw cycles. Our results revealed low electrical resistivity (<20 Ωm) and elastic moduli (7.7 GPa for Young's modulus and 2.9 GPa for shear modulus) at temperatures down to ~−10 °C, indicating the presence of a significant amount of unfrozen saline water under the current field conditions. The spectral induced polarization signal showed a systematic shift during the freezing process, affected by concurrent changes of temperature, salinity, and ice formation. An anomalous induced polarization response was first observed during the transient period of supercooling and the onset of ice nucleation. Seismic measurements showed a characteristic maximal attenuation at the temperatures immediately below the freezing point, followed by a decrease with decreasing temperature. The calculated elastic moduli showed a non-hysteric response during the freeze – thaw cycle, which was different from the concurrently measured electrical resistivity response where a differential resistivity signal is observed depending on whether the soil is experiencing freezing or thawing. The differential electrical resistivity signal presents challenges for unfrozen water content estimation based on Archie's law. Using an improved formulation of Archie's law with a variable cementation exponent, the unfrozen water content estimation showed a large variation depending on the choice of the resistivity data during either a freezing or thawing cycle. Combining the electrical and seismic results, we suggest that, rather than a large hysteresis in the actual unfrozen water content, the shift of the resistivity response may reflect the changes of the distribution pattern of the unfrozen water (or ice) in the soil matrix during repeated freeze and thaw processes. Collectively, our results provide an improved petrophysical understanding of the physical and mechanical properties of saline permafrost during freeze – thaw transitions, and suggest that large uncertainty may exist when estimating the unfrozen water content using electrical resistivity data.


## 1. Introduction

Saline permafrost is widespread both onshore and offshore in the Arctic region (Hivon and Sego, 1993; Humlum et al., 2003; Krylov and Bobrov, 1998; Osterkamp, 2001). It is defined as perennially subzero temperature soil with pores filled by high-salinity water that remains partially unfrozen at temperatures below 0 °C due to freezing point depression (Banin and Anderson, 1974; Marion, 1995). While most of the unfrozen water in freshwater permafrost soils exists as surface-bound water and thin water films in the vicinity of soil grains, unfrozen water in saline permafrost could also occupy the bulk pore space (Hivon and Sego, 1995). The unfrozen water content in saline permafrost can fluctuate significantly during freeze – thaw transitions with temperature change, and is the dominant factor controlling its mechanical and hydrological properties. Nixon (1987) demonstrated dramatic reduction in the mechanical strength of saline permafrost at subzero temperature with pile load tests. Hivon and Sego (1995) observed significant loss of strength of saline permafrost at subzero temperatures when compared with less saline soils. The compromised mechanical strength of saline permafrost could have a significant impact on infrastructure stability built on permafrost soils (Hivon and Sego, 1995; Brouchkov, 2003).

Geophysical methods, such as electrical and seismic methods, have been widely used in permafrost research at both lab and field scales to estimate the unfrozen water content of permafrost and its implications on permafrost physical and mechanical properties (Dou et al., 2016, 2017; Dafflon et al., 2016; Wu et al., 2013; French et al., 2006; Krautblatter and Hauck, 2007; Oldenborger and LeBlanc, 2015). Significant contrasts in electrical resistivity and elastic properties between frozen and unfrozen soil are the basis for these methods. For example, while unfrozen soils have a typical resistivity value from a few to hundreds of ohm-meters depending on pore water salinity, saturation, soil type and texture, typical resistivity for frozen soils ranges from tens to

* Corresponding author.
*E-mail address:* YWu3@lbl.gov (Y. Wu).

http://dx.doi.org/10.1016/j.jappgeo.2017.08.008

hundreds of kilo-ohm-meters (French et al., 2006; Krautblatter and Hauck, 2007; Fortier et al., 2008; Dafflon et al., 2013; Wu et al., 2013), with the except of soils with high clay contents. While studies on freshwater permafrost are extensive, similar studies on saline permafrost are limited. Due to freezing point depression, unfrozen water content in saline permafrost is expected to be considerably higher than its freshwater counterparts under the same temperature and texture conditions, resulting in vastly different geophysical and mechanical properties and behaviors. In addition, hysteresis in unfrozen water content during the freeze – thaw cycles of frozen soils has been known for permafrost soil due to metastable ice nucleation as well as capillary and adsorption effects (Bittelli and Flury, 2003; Ishizaki et al., 1996; Tian et al., 2014). Most of these studies focus on freshwater soils, generally showing a higher unfrozen water content during the freezing than the thawing cycle, and studies for saline permafrost are sparse. If hysteresis exists in saline permafrost, how it affects its geophysical and mechanical properties are important for the development of geophysical permafrost monitoring methods.

In this research, we present a laboratory study to understand geophysical properties of saline permafrost soils during freeze-thaw cycles, and their implications for the estimation of unfrozen water content and the soil's physical and mechanical properties. We acquired the saline permafrost soils from a site in Barrow, AK, ~300 miles north of the Arctic Circle. Multiple geophysical (electrical, seismic and electromagnetic) surveys at this site have identified an extensive saline permafrost layer overlain by a shallow active layer and freshwater permafrost (Hubbard et al., 2013; Dou and Ajo-Franklin, 2014). This saline permafrost layer, characterized by low resistivity in the range of a few to tens of Ωm, may be less than two meters below ground surface in some locations, confirmed by coring.

During the experiment, we conducted electrical resistivity, spectral induced polarization (SIP), and low- (sonic-) frequency seismic measurements (Young's, **E**, and shear, **G**, modulus). To the best of our knowledge, low frequency (<1000 Hz) SIP signals of natural saline permafrost soils during freeze – thaw transition has not been explored and how changes of temperature, unfrozen water content, salinity and ice formation collectively impacts its SIP response is not well understood. In addition, we discussed how electrical resistivity measurements were used to estimate the unfrozen water content and proposed a modified formula based on Archie's law. Specifically, we took into account the changes of the soil cementation factor due to soil structural change induced by ice formation and the effect of temperature and increase in salinity on fluid conductivity of the unfrozen water explicitly. We evaluated the uncertainty of unfrozen water content estimation based on Archie's law during freeze – thaw cycles. For seismic monitoring, while most of previous seismic studies on permafrost were conducted at ultrasonic frequency range, our sonic frequency seismic measurements offered several advantages. First, the wavelengths at sonic frequencies were much large, therefore its velocity and attenuation were less affected by wave scattering from soil grains, fluid/ice inclusion and layer heterogeneity. Second, seismic velocity dispersion and attenuation are inherently frequency dependent, therefore it is desirable to conduct laboratory measurements with frequencies close to those used in the field to help with field data interpretation. Co-collection of both electrical and seismic data allowed joint data interpretation, which lead to better understanding of the physical and mechanical processes in the saline permafrost soil during the freeze - thaw process.

## 2. Electrical and seismic methods for saline permafrost studies

Multiple geophysical methods have been used for permafrost studies. Numerous studies have used both ground-based and airborne electrical resistivity and electromagnetic surveys to explore resistivity contrasts to delineate permafrost structures and dynamics over time and space. For example, Minsley et al. (2012) conducted airborne electromagnetic surveys to map permafrost distribution in the Yukon flats region. Hubbard et al. (2013) combined ground based Electrical Resistivity Tomography (ERT) with remote sensing and point based measurements to explore permafrost zonation and correlations with biogeochemical properties. Dafflon et al. (2016) used ERT to estimate shallow permafrost distribution in an ice-wedge polygon dominated arctic tundra. Hilbich et al. (2008) conducted ERT survey of a mountain permafrost and identified the dynamics of active layer thickness over time. Krautblatter and Hauck (2007) and Krautblatter et al. (2010) conducted ERT surveys of permafrost rock walls to study temperature effects on permafrost dynamics in order to evaluate its mechanical stability based on laboratory calibrated temperature – resistivity correlation. Fortier et al. (2008) combined ERT survey with field temperature logging, cone penetration tests and core logging to study the internal structure of permafrost mounds.

All studies confirm that temperature has a significant effect on electrical resistivity in permafrost. However, while a linear correlation between temperature and resistivity is widely observed for unfrozen soils at temperature above 0 °C (Hayley et al., 2007; Krautblatter and Zisser, 2012), both linear and exponential correlations have been observed for partially frozen soils (Hayley et al., 2007; Krautblatter and Zisser, 2012; Wu et al., 2013). This is possibly related to soil texture, especially tightness and interconnectedness of water saturated pores (Krautblatter and Zisser, 2012).

In addition to resistivity, induced polarization (IP, in forms of single frequency, spectral IP or complex resistivity) signals have also been explored to study permafrost (Frolov, 1973; Olhoeft, 1977; Krylov and Bobrov, 1998; Wu et al., 2013; Banville et al., 2016). Frolov (1973) studied the elastic and electrical signals of frozen ice and soils and showed the effects of soil texture, moisture content and temperature on these properties. Specifically, dielectric measurement at frequencies >3 K Hz shows that the electrical properties of the frozen soil are determined by the specific surface area of the soil, the ice and unfrozen water content. Similar studies by Maeno et al. (1992) also found the unfrozen water weakly bounded on mineral surface generates large dielectric polarization and conduction. Olhoeft (1977) studied the complex resistivity behavior of clay-rich permafrost and observed strong frequency-dependent behavior of the complex resistivity at frequencies above 10 Hz. Olhoeft (1977) suggested a few different mechanisms responsible for the observed electrical behavior that include ionic conduction, a Maxwell–Wagner type of effects, Bjerrum defects (Bjerrum, 1952) as well as the relaxation of unfrozen water molecules in the soil. Grimm et al. (2008) and Stillman et al. (2010) studied the induced polarization signals of silicate – ice mixtures. They also observed strong frequency dependent behavior of the electrical signals that are related to these effects. Fortier and Allard (1998) identified IP anomaly at the boundary between frozen and unfrozen layer that is likely relevant to interfacial Maxwell–Wagner effects. Wu et al. (2013) explored low frequency electrochemical IP effects of permafrost soils. They observed an increase of the polarization signal during isothermal thawing at 0 °C which are related to the increase of the unfrozen soil grains and pore fluid. Krylov and Bobrov (1998) performed field studies of the saline permafrost on the Yamal Peninsula in Russia and identified different soil layers having different soil texture and ice content with resistivity. They also observed polarization anomalies that were attributed to the existence of frozen saline clay. In addition to vertical profiling, induced polarization tomography has been used for periglacial studies in recent years (Banville et al., 2016). Studies by Grimm et al. (2008) and Stillman et al. (2010) on artificial mixtures of silicate with saline proposed multiple polarization mechanisms that are linked with the different structural components of the mineral-ice-brine system. This includes contributions from both low frequency diffusive and Maxwell–Wagner type of polarization to higher frequency ice polarization and polarization associated with surface absorbed water.

Seismic velocity and attenuation of permafrost, frozen soils or gas hydrates have also been studied in both laboratory and field. Kurfurst

(1976) conducted ultrasonic P- and S-wave measurements on natural permafrost samples from several sites. The laboratory measured velocities were in reasonable agreement with the field seismic surveys, providing confidence in interpretation of field data using laboratory measurements. Dou et al. (2016, 2017) conducted laboratory studies on unconsolidated saline permafrost and developed an effective-medium model to explain the observed P wave velocity changes during the freeze – thaw transition. Dou and Ajo-Franklin (2014) conducted field based seismic measurements in the arctic permafrost region and identified low P wave velocity zones that is likely due to the presence of partially frozen saline permafrost, consistent with previous findings with electrical measurements (Hubbard et al., 2013). King et al. (1988) also conducted ultrasonic (500 kHz–850 kHz) measurements on permafrost samples and applied the Kuster-Toksoz model (Kuster and Toksoz, 1974) to predict P- and S-wave velocities of permafrost, by sequentially modeling the unfrozen water and then solid grain as spherical inclusions. The model was used to explain P- and S-wave velocity changes at ultrasonic frequencies, and then to determine the unfrozen water content of the permafrost. In addition to laboratory studies, field scale seismic surveys have been conducted to characterize frozen materials. For example, borehole based P- and S- wave velocity measurements were used to estimate gas hydrate concentrations (Carcione and Gei, 2004).

In contrast to the velocity, attenuation behavior of partially frozen permafrost has not been well documented. Matsushima et al. (2008) conducted ultrasonic P-wave attenuation measurements in partially frozen pure brines. They observed large increases in the attenuation at temperatures immediately below the freezing/melting point. This effect was also observed in ultrasonic P-wave measurements in partially frozen orange juice (Lee et al., 2004), which was explained by Biot's model (Carcione et al., 2007). A part of the observed changes in the attenuation of the ultrasonic waves, however, may be attributed to the scattering of the waves by ice inclusions. Spetzler and Anderson (1968) conducted longitudinal and torsion resonant bar tests on pure water-ice rods and 1% and 2% brine ice rods, at frequencies less than ~5 kHz. Because of the long wavelengths of the measurements, the measured attenuation can be interpreted as the intrinsic attenuation. At permafrost temperatures above the eutectic point, measurements of the fundamental resonance modes indicated that both longitudinal and torsion attenuation increase monotonically with increasing temperature.

## 3. Archie's law for unfrozen water content estimation

As discussed above, unfrozen water content is the dominant factor controlling the mechanical and physical properties of permafrost soil. The unfrozen water content in partially frozen soils is routinely estimated using geophysical methods, relying on the sensitivity of geophysical attributes, e.g. dielectric constant or $T_2$ magnetic relaxation, to unfrozen water content. Nuclear magnetic resonance (NMR) and Time Domain Reflectometry (TDR) are among the most popular methods (Hivon and Sego, 1995; Ishizaki et al., 1996; Jahnert et al., 2008; Patterson and Smith, 1984; Smith and Tice, 1988; Stillman et al., 2010; Watanabe and Mizoguchi, 2002).

While both NMR and TDR methods yield reasonable unfrozen water content estimation, they are difficult to use at field scales to provide enough spatial coverage, particularly when significant variability of unfrozen water is present. Alternatively, electrical resistivity measurements have been used to estimate unfrozen water content in partially frozen soils based on Archie's law (Daniels et al., 1976; Hauck, 2012; King et al., 1988; Scherler et al., 2011). At field scales, the electrical resistivity method is advantageous because resistivity measurements can be collected relatively easily and autonomously at large scales.

Most studies for unfrozen water content estimation based on resistivity were conducted on freshwater soils and they generally assume a fixed cementation exponent ($m$) and saturation exponent ($n$) values in Archie's law (Archie, 1942):

$$\rho_{bulk} = \rho_w \phi^{-m} S_w^{-n} \tag{1}$$

where $\rho_{bulk}$ is the bulk resistivity, $\rho_w$ represents fluid resistivity, $\phi$ is porosity and $S_w$ is saturation.

$S_w$ is generally treated as the variable to represent the unfrozen water content while the porosity ($\phi$) is considered constant. Archie's law has been simplified to the following form for unfrozen water content estimation (Daniels et al., 1976).

$$\frac{\rho_f}{\rho_\tau} = S_w^{1-n} \tag{2}$$

where $\rho_f$ is the resistivity of the frozen soil at a given temperature, and $\rho_t$ is the resistivity of the same soil when it is completely unfrozen.

While Eq. (2) provides simplicity, it does not consider soil structure changes during ice formation as well as the effect of temperature change on the conductivity of the unfrozen water (King et al., 1988). Here, we provide a different application of Archie's law by explicitly representing soil structural changes due to ice formation and the effects of changes in temperature and salinity on conductivity of the unfrozen water.

First, we treat the porosity $\phi$ (instead of water saturation $S_w$) as the variable to represent unfrozen water content in the partially frozen soil. Essentially, instead of treating the ice as an equivalent of air that causes "desaturation" (decrease of $S_w$), the ice is treated as a new solid phase that reduces porosity, $\phi$ (i.e. structural changes). For fully saturated soils, $S_w$ equals to 1 and can be eliminated from Eq. (1). Secondly, we treat the cementation exponent $m$ as a variable instead of keeping it fixed during ice formation. Physically, this is reasonable because $m$ represents the "cementation" or "tightness" of the soil matrix (Glover, 2009), thus as ice forms and fills the pore spaces we can expect some increase of the "cementation" or "tightness" of the soil. Third, we exclusively represent pore fluid conductivity change by including (Archie, 1942) the effect of salinity increase in the unfrozen water due to salt exclusion and (Banin and Anderson, 1974) the concurrent temperature coefficient of fluid conductivity.

With these considerations, we have

$$\sigma_w^T = \sigma_w^{T_0}\left(\frac{\phi^{T_0}}{\phi}\right)[1-\alpha(T_0-T)] \tag{3}$$

$$\sigma_w^T = \frac{1}{\rho_{bulk}^T \phi^m} \tag{4}$$

where $\sigma^T{}_w$ represents fluid conductivity of the unfrozen water at a given temperature $T$. $\rho^T{}_{bulk}$ is the bulk resistivity of the frozen soil at this same temperature. $\alpha$ is the fluid conductivity temperature coefficient (typical value ~2.1%). $T_0$ is a reference temperature when the soil is completely unfrozen. $\sigma^{T0}{}_w$ and $\phi^{T0}$ represent fluid conductivity and porosity at $T_0$. Combining Eqs. (3) and (4), we have

$$\phi = \left[\rho_{bulk}^T \sigma_w^{T_0} \phi^{T_0}(1-\alpha(T_0-T))\right]^{\left(\frac{1}{1-m}\right)} \tag{5}$$

Eq. (5) provides an alternative formula for unfrozen water content estimation based on the bulk soil resistivity measurements.

## 4. Materials and methods

### 4.1. Experimental procedure

The saline permafrost soil was acquired from the NGEE-Arctic (Next Generation Ecosystem Experiments - Arctic) site, located in the Barrow

Environmental Observatory (BEO) in Barrow, AK. It is a region with continuous permafrost typified by a few dominant geomorphic features, including polygonal ground, thaw lakes and drained thaw lake basins of different ages.

Coring for the saline permafrost soil was conducted when the ground temperature was still below 0 °C and the surface soil was frozen. The core used for the experiment was collected in the center of a flat centered polygon where extensive and very shallow saline permafrost has been identified by ERT and seismic surveys (Hubbard et al., 2013; Dou and Ajo-Franklin, 2014). Soil at the bottom of the core from 260 to 280 cm below ground surface was identified as saline permafrost and used in this study. The fluid conductivity of the extracted pore water was ~6.23 S/m at room temperature (23 °C) with an estimated salinity at ~45 parts per thousand (PPT), higher than that of typical sea water (~35 PPT). The bulk density of the soil was ~2.11 g/cm$^3$ and the porosity was ~33% based on gravimetric measurements. For the laboratory experiments, the soil was repacked into a smaller cylindrical core in a polyvinyl chloride (PVC) sleeve (height 7.55 cm, diameter 3.81 cm). The repacked sample was close to full saturation before experiment started based on density calculation and X-ray Computed Tomography (CT) scans. Particle size analysis shows that this soil contains <4% clay with ~30% of soil grains between 2 and 50 μm and 64% between 50 and 250 μm in size.

The experiment was conducted in an incubator under controlled temperature conditions. The soil core was frozen down to ~−9 °C during the initial freezing phase. Subsequently, the temperature of the soil was increased step wisely up to +7 °C over a 5 day period (the heating rate varied between the temperature intervals, but typically slower than 0.5 °C/h to ensure quasi-steady state). The temperature of the soil core was monitored with thermocouples. Subsequently, a refreezing stage of the experiment was conducted following the same procedure as the thawing stage. Throughout the initial freeze - thaw - refreeze cycle, electrical data were collected continuously using an automated system, and seismic measurements were made manually and only in the thaw – refreeze phase.

### 4.2. Experimental setup

The experimental setup used for the freeze - thaw tests with concurrent electrical and seismic measurements is shown in Fig. 1. This setup used a variant of the Split Hopkinson Resonant Bar apparatus (Nakagawa, 2011) which allows sonic-frequency-range seismic measurements of short core samples. The apparatus used in the current experiment employed a pair of vertical stainless steel rods as end plugs for a jacketed soil core, which also reduced the acoustic (seismic) resonance frequencies of the entire setup. A seismic source unit containing both compression and torsion piezoelectric elements was attached to the far end of the bottom rod, and a vertical accelerometer (for compression or longitudinal motions) and a pair of lateral accelerometers (for torsion motions) to the top end of the top rod. The sample jacket was a semi-rigid, heat-shrink PVC tube (thickness 0.5 mm). To reduce acoustic coupling, the entire setup was suspended in an acrylic cage using a pair of steel wires and springs attached to the near-sample end of the bottom rod. This also facilitated electrical isolation of the two steel rods at the both ends of the sample. Although the experiment was conducted without applying confining stress or pore pressure to the sample, the mass of the rod on top of the sample resulted in 4.57 psi (31.6 KPa) of stress.

### 4.3. Electrical data acquisition

For electrical resistivity data acquisition, the stainless steel rods in direct contact with the end faces of the soil were used for current injection and two Ag/AgCl electrodes installed in the middle of the soil core were used for electrical potential measurements. A data acquisition system based on National Instrument signal analyzer (NI 4461) was

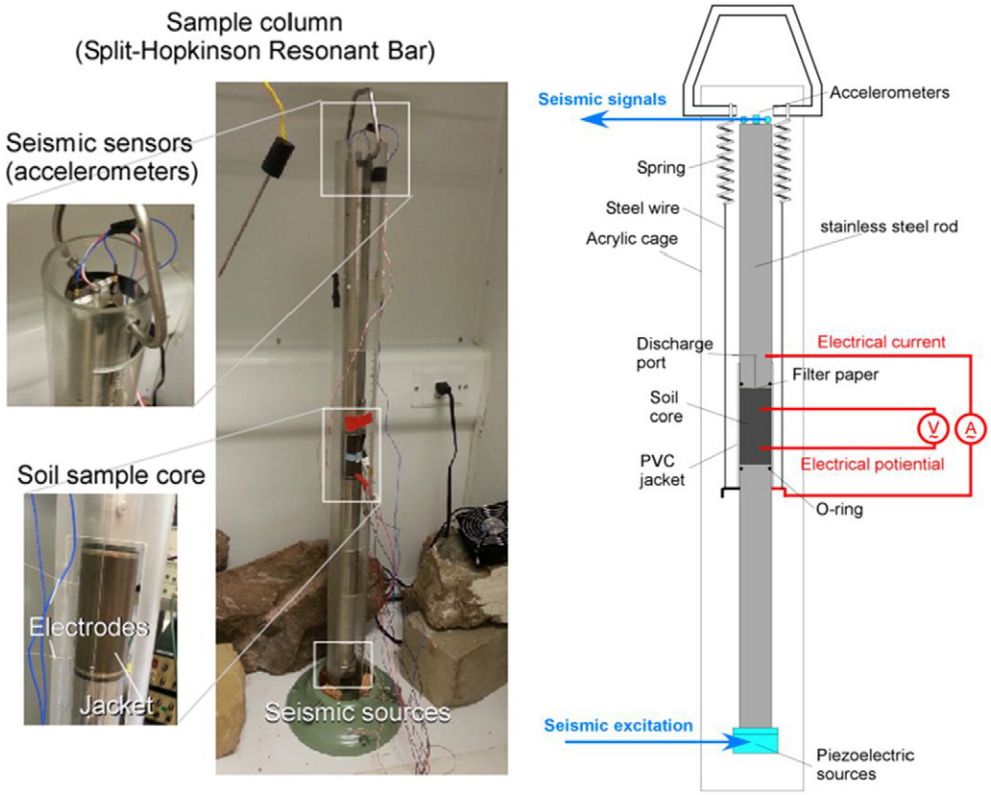


**Fig. 1.** Experimental setup for the freeze-thaw experiment with concurrent electrical and seismic measurements.

used for electrical data acquisition in the frequency range from 1 to 1000 Hz. The complex electrical data can be present in forms of complex resistivity ($\rho^*$), conductivity ($\sigma^*$) or dielectric permittivity ($\varepsilon^*$). In terms of conductivity, its real ($\sigma'$) and imaginary ($\sigma''$) components can be calculated based on a conductivity magnitude ($|\sigma|$) and a phase shift ($\phi$) term that are outputs from the data acquisition system using the following equations:

$$\sigma' = |\sigma| \times \cos\phi \tag{6}$$

$$\sigma'' = |\sigma| \times \sin\phi \tag{7}$$

The conversion between $\rho^*$, $\sigma^*$ and $\varepsilon^*$ are as follow:

$$\sigma^* = \frac{1}{\rho^*} = i\omega\varepsilon^* = \sigma'(\omega) + i\sigma''(\omega) \tag{8}$$

The electrical signal from most soils is a complex term that exhibits some degree of frequency dependence. While the real component of the electrical signal measures the ability of the soil to conduct (or impede) flow of electrical charges, the imaginary component is linked to the charge polarization that predominantly occurs at the mineral-electrolyte interface at low frequencies in natural soils. Soil porosity, permeability, mineralogy, pore fluid saturation, salinity and temperature are all factors affecting the magnitude of both the real and imaginary electrical signals. While electrical charge conduction occurs through both interconnected pore space and the mineral surface, the low frequency polarization signal is primarily an electrochemical phenomena occurring in the electrical double layer (EDL) at the mineral - electrolyte interface. For saline soil with high pore fluid salinity, because the EDL at the mineral - electrolyte interface is strongly compacted based on the Guoy - Chapman model (Stumm and Morgan, 1996), its contribution to the overall electrical conductivity can be ignored when compared with the contribution from conduction through the pore space. The impact of salinity on charge polarization is more complicated. While the charge polarization component has been observed to increase when pore fluid salinity is increased moderately, higher pore fluid salinity (e.g. when fluid conductivity is higher than a few Siemens per meter) tends to reduce the polarization magnitude and increase the relaxation time constant due to the reduced mobility of charged ions in the EDL when the adsorption sites are saturated (Lesmes and Frye, 2001; Slater et al., 2005; Kruschwitz, 2008).

The effects of temperature change on the electrical signals during the freeze - thaw cycle of saline soil need to be investigated due to its effects on both resistivity and induced polarization signals. While the effect of temperature on resistivity has been demonstrated repeatedly, its effects on low frequency electrical polarization has only been observed by limited studies on sandstone or shaly sand samples at temperatures above 0 °C (Vinegar and Waxman, 1984; Worthington and Collar, 1984; Tong and Tao, 2007; Zisser et al., 2010). In most cases the increase of the polarization signal and decrease of the relaxation time constant were observed with increasing temperature which is attributed to the increases of both charge mobility and density at higher temperatures (Zisser et al., 2010). The effects of temperature on the induced polarization signal of freezing natural saline soil are not well understood.

In addition to temperature, it is well known that Bjerrum defects can cause electrical polarization in ice (Bjerrum, 1952; Petrenko and Whitworth, 1999). Depending on temperature and the abundance of defects, the relaxation frequencies of this polarization mechanism are normally above 100 Hz (Stillman et al., 2010). Stillman et al. (2010) observed an increase of the ice relaxation frequency with decreasing ice concentration which they attribute to an increasing density of lattice defects when ice fills a smaller portion of the pore space.

### 4.4. Seismic data acquisition

Seismic data acquisition was conducted by applying chirp vibrations (sine wave sweeps with a monotonically increasing frequency) to the sample in either longitudinal or torsion mode sequentially. The source signal was produced by a spectrum analyzer (ONNO-SOKKI CF6400), amplified by a wide-band amplifier (Krohn-Hite 7602M), and applied to the piezoelectric elements. The resulting vibration signals were sensed using accelerometers (PCB Piezotronics, 352C22 for torsion, 352C67 for longitudinal), conditioned (via PCB signal conditioner 482C), stored and analyzed by the spectrum analyzer.

The raw data obtained from the seismic measurements are the longitudinal and torsion resonance frequencies, and the attenuation (damping) of the related resonances determined via the half-power method. Because the measured resonances are for the entire experimental setup (i.e., steel rods, sample, jacket, source unit, and sensors, etc.), a numerical model is used to extract the complex elastic moduli of the sample via inversion. These are the (complex valued) Young's modulus and shear modulus of the sample, corresponding to the longitudinal and torsion vibration measurements, respectively. Inversion for the elastic modulus can be affected by the torsion vibration measurement as well, depending upon the Poisson ratio of the sample and the sample end-constraint effect (Nakagawa, 2011).

In principle, with the knowledge of the sample density, P- and S- wave velocities and attenuations can be determined from these measurements. However, for samples with a large Poisson ratio, errors in determining the P-wave velocity and attenuation become very large (Winer and Nur, 1979). Additionally, for very compliant samples, such as unconsolidated sand and soil, the stiffness of the jacket can exceed that of the sample, which introduces additional errors in both inverted P- and S-wave properties. For these reasons, in this paper, we will not present P- and S-wave properties as the results of the seismic measurements. Instead, we will show Young's modulus and shear modulus as their proxies, which are more directly related to the actual measured quantities (longitudinal and torsion resonances, respectively) and less susceptible to errors.

### 4.5. CT scans

The permafrost sample was scanned by X-ray computed tomography using a modified medical General Electric Lightspeed 16 CT scanner before the test, immediately upon refreezing the sample following the freeze-thaw test, and following a later deep freeze to −80 °C. CT scans were used to evaluate whether significant structural changes occurred during the freeze - thaw processes that could have dramatic impacts on the geophysical measurements. Cross sections of the cylindrical sample prior to the freeze-thaw test, immediately following the test, and following the post-test deep freeze are presented in Fig. 2. The sample was initially 37.5 mm in diameter and 76 mm long. Several small low-density regions scattered throughout the sample are apparent in Fig. 2A, B and C. The density in these “voids” exceeds 1, indicating that they are filled with water-saturated, poorly compacted sediment. Over the duration of the test, the size of these low-density regions decreased (note size difference between the dark spots in Fig. 2A and B). CT scans are calibrated to density using a calibration curve created from scanning a number of cylindrical objects of known density (air, water, acrylic, nylon, glass, 6061 Al). The mean density of the sample computed from X-ray CT for each of the conditions shown was 2.11 g/cm$^3$ (pre-test), 2.23 g/cm$^3$ (post-test), and 2.18 g/cm$^3$ (deep freeze), consistent with those measured gravimetrically. Following the freeze-thaw test, the sample diameter was approximately the same, but the length decreased slightly to 75 mm. This is within the error of measurement for the CT scanner for the applied conditions, as the presence of the resonance bars after the test causes severe artifacts in the end CT slices which are 0.625 mm thick.

Sample packing imparted a slight anisotropic structure to the medium. This structure manifests itself as higher (~2.27 g/cm$^3$) and

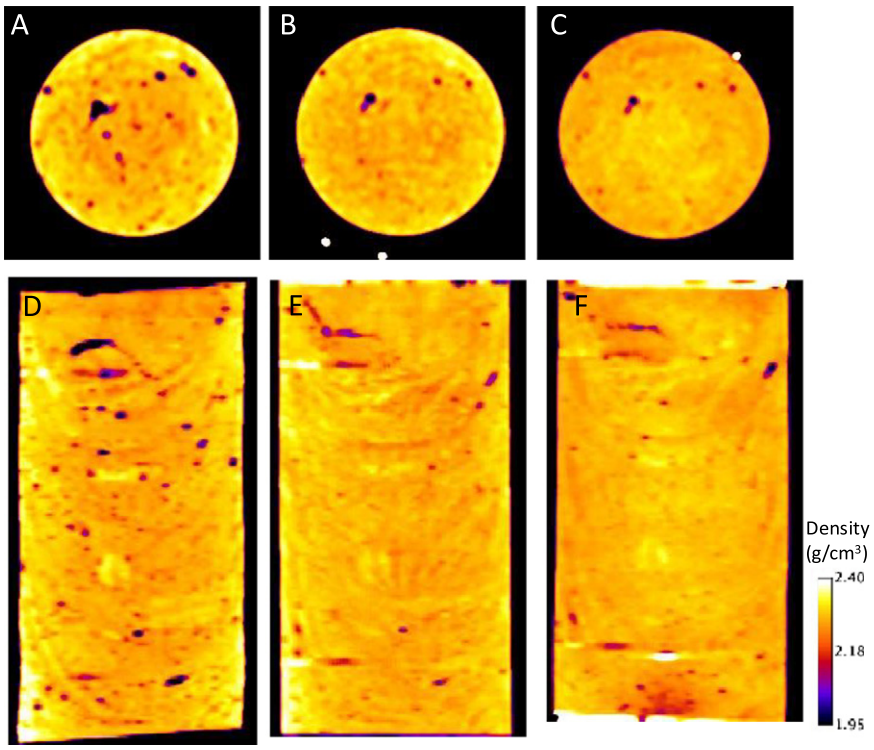


**Fig. 2.** CT cross sections of the sample from approximately the same location: (A, D) before the test (thawed), (B, E) after the test (frozen), and (C, F) after deep freeze (frozen).

lower (~2.21 g/cm$^3$) density bands that curve upwards in Fig. 2D, E and F. A few high-density grains (2.5 g/cm$^3$) <7 mm in size were also observed. Ice veins similar to those observed in other freeze tests were not observed in this test under either of the freezing conditions (Kneafsey et al., 2011).

## 5. Results and discussion

The datasets presented in this research are available online (Wu et al., 2017, http://dx.doi.org/10.5440/1374172).

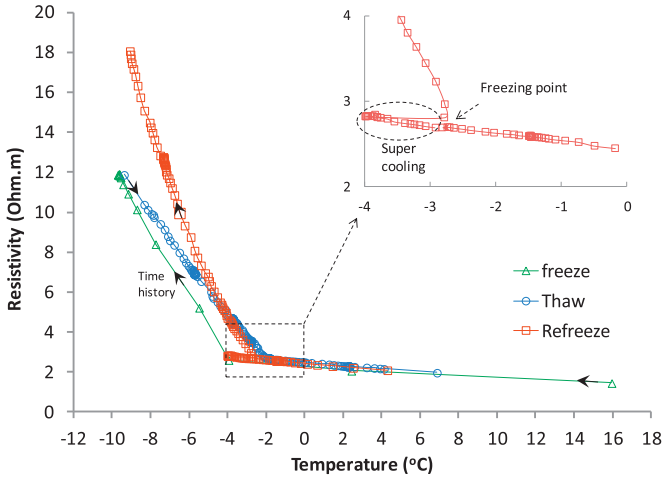


**Fig. 3.** Electrical resistivity changes in responding to soil temperature variation during the freeze (green) – thaw (blue) – refreeze (red) cycles. The arrows indicate the time history of the data points. The insert demonstrates the freezing point depression and the supercooling effect during refreezing.

### 5.1. Electrical resistivity

Changes of electrical resistivity during the initial freeze – thaw – refreeze circle of the experiment are shown in Fig. 3, where a strong shift of the electrical signal is observed at ~−2 to −3 °C.

While resistivity at temperatures above −2 °C is nearly identical for all three different test phases (initial freeze, thaw, refreeze), large difference in resistivity is apparent for temperatures below −2 °C. Except for temperatures from ~−2 °C to −4 °C in the refreeze phase, there is an upward shift of the resistivity curves at temperatures below −2 °C if one follows the time history of the experiment.

A common characteristic during all three phases of the experiment is the resistivity inflection between −2 °C and −4 °C, marked by a steeper slope in resistivity – temperature correlation at lower temperatures. This is the freezing point of the saline permafrost soil. As mentioned above, the presence of salt in the pore fluid depresses its freezing point and the freezing point of a saline soil can be estimated based on the follow empirical equation presented in Potter et al. (1978):

$$T_{fp} = 0.00 + 0.581855S_n + 3.48896 \times 10^{-3}S_n^2 + 4.314 \times 10^{-4}S_n^3 \quad (9)$$

where $T_{fp}$ is the freezing point depression in °C, $S_n$ is salinity in weight percent of salt in solution. Based on Eq. (9), the initial freezing point of our saline permafrost soil should be ~−2.7 °C, which is in good agreement with the observed value in the experiment (inserted subfigure in Fig. 3).

Ice starts to form when temperature drops below the freezing point. As a result, the fraction of the pore space occupied by unfrozen water is reduced, generating a positive feedback to the bulk resistivity because ice can be considered an electrically insulating material when present in saline fluids. However, salt exclusion occurs concurrently during ice formation, which increases the salinity, therefore conductivity, of the remaining unfrozen water, generating a negative feedback to the resistivity of the bulk material. The competing effects of these two dictate the overall change of the resistivity during freezing of saline

soil and Fig. 3 suggests a more dominant effect on resistivity from ice formation. One should also note that temperature change itself has an effect on resistivity and requires consideration as well. In fact, the resistivity change at temperatures above ~−2 °C (before freezing occurs) shown in Fig. 3 is a pure temperature effect and follows a linear resistivity – temperature correlation with a slope of ~3.6% bulk resistivity change per °C for this saline permafrost soil.

While the resistivity – temperature correlation above −2 °C is nearly identical for the three freeze thaw phases and can be adequately explained by temperature, the large differences in resistivity at below −2 °C indicate possible difference in the unfrozen water content and/or the pattern of ice formation and distribution during repeated freeze thaw processes. While these processes are better explained together with the seismic data, thus will be discussed later, we note that the resistivity at ~−9 °C are still extremely low (<20 Ω·m) for all three phases, indicating the possible high unfrozen water content in the soil. We will discuss this separately later.

Supercooling (Velli and Grishin, 1982) was observed in the experiment. While sparse data density prohibits the observation of this phenomenon during the initial freezing cycle, such an effect is clearly shown during the refreeze cycle when much higher temporal data density is available (inserted subfigure in Fig. 3). The supercooling effect is characterized by an initial ice nucleation temperature (−4 °C in this experiment) below the freezing point (−2 °C), and small transient increase of temperature during ice nucleation due to heat release. We note that supercooling is a metastable state present only at the initiation of ice nucleation and should not be confused with freezing point depression.

In addition to the electrical resistivity signal discussed above, induced polarization signals collected during the freeze - thaw transition also showed characteristic changes (Fig. 4). Fig. 4A shows a systematic shift of the phase shift spectrum during the freezing process that includes (Archie, 1942) a consistent decrease of the phase magnitude in general for frequency <100 Hz; (Banin and Anderson, 1974) a consistent increase of the phase magnitude for frequencies >100 Hz and (Bjerrum, 1952) a shift of the peak phase frequency to lower values across the whole spectrum. The low frequency (<100 Hz) polarization signals are likely due to diffusive or Maxwell–Wagner type relaxation associated with charged ions in the vicinity of the mineral surface, and the increase of the phase response at frequencies >100 Hz could be related to the dielectric relaxation of ice associated with Bjerrum defects as suggested by Stillman et al. (2010). Although the whole ice relaxation spectrum at >1000 Hz was not captured within the frequency range measured during the experiment, the increase of the magnitude of this polarization effects seem to associate with a shift of the spectrum toward lower frequencies with decreasing temperature, i.e., increasing ice content, which is consistent with the observations made by Stillman et al. (2010). The changes of the imaginary conductivity spectrum are similar to the phase shift spectrum and not shown.

We attribute the changes of the polarization signal at <100 Hz to changes in temperature and salinity during progressive ice formation that affects diffusive polarization along mineral surface. Similar temperature effects on induced polarization have been observed by Zisser et al. (2010), but in different systems at temperatures above 0 °C. Briefly, the decrease of temperature is accompanied by a decrease of the overall polarization magnitude as well as a decrease of the peak frequency (i.e. an increase of the relaxation time constant, a parameter derived from Cole – Cole type of models). Zisser et al. (2010) attribute these changes to temperature effects on EDL charge mobility as well as charge density. Specifically for the saline permafrost soils, decreased temperature could decrease charge mobility and charge density during the freezing process, and result in the observed shift of the spectral electrical responses to lower frequencies shown in Fig. 4A. In addition to the temperature effects, the increase of salinity of the unfrozen water film due to salt exclusion during ice formation could also contribute to the decrease of the polarization magnitude through reducing the EDL thickness and the increase of relaxation time through the reduced mobility of the charged ions as discussed above.

When examining the correlation between temperature and the polarization signal (imaginary conductivity and phase shift) at 1 Hz (Fig. 4B), transient polarization anomaly at temperature from ~−2 °C to −4 °C within the general decreasing trend of the polarization signal with deceasing temperature is apparent. This coincides with the observed transient supercooling effect and the abrupt temperature changes associated with the initiation of ice nucleation. While this polarization anomaly could be due to these changes, the underlying mechanism is unclear.

### 5.2. Seismic data

Seismic measurements were conducted concurrently with the electrical measurements, during the freeze-thaw experiment. Changes in the Young's modulus (E) and shear modulus (G) and their related attenuations ($1/2Q_E$ and $1/2Q_G$ where Q is the seismic quality factor) are shown as a function of the temperature in Fig. 5. These results were corrected for the PVC jacket confining the sample. Although the modulus of the jacket were measured independently at comparable frequencies (~100–300 Hz) (data not shown), because the jacket's thickness can be uneven around the sample, the error bars were computed for ±10% changes in the stiffness of the jacket.

Different from the large differences in the electrical signal between the freezing and thawing phases, the elastic moduli increased linearly with decreasing temperature starting from onset of freezing, exhibiting only small differences during the freezing Vs thawing phases (Fig. 5A). Maximum values of ~7.7 GPa and 2.9 GPa for the Young's and shear modulus were observed at ~−9 °C. Our experiment did not reach the eutectic temperature where all the pore fluid freeze or crystallize. However, Dou et al. (2016, 2017) conducted ultrasonic P-wave

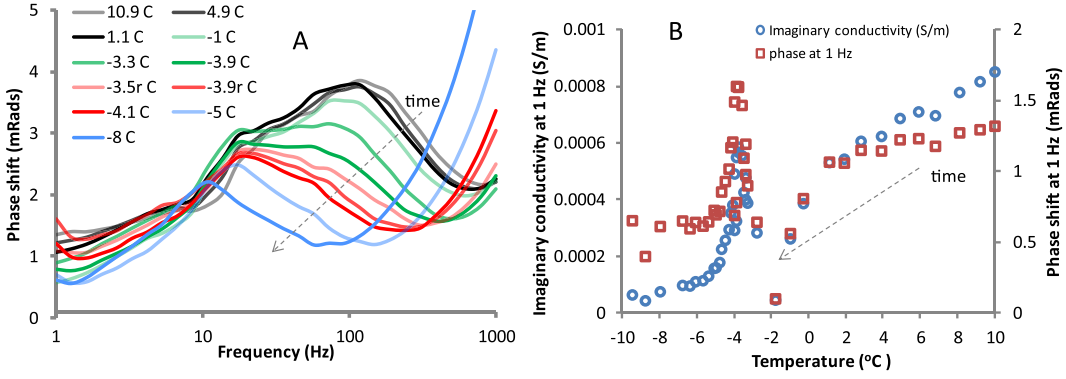


**Fig. 4.** Electrical polarization signal changes during freeze – thaw transitions. (A) Spectral (1–1000 Hz) phase shift change during the freezing process from +10 °C to −8 °C (−3.5r and −3.9r represents transient temperature rebound during onset of ice nucleation); (B) imaginary conductivity and phase shift at 1 Hz during the freezing process of the saline soil.

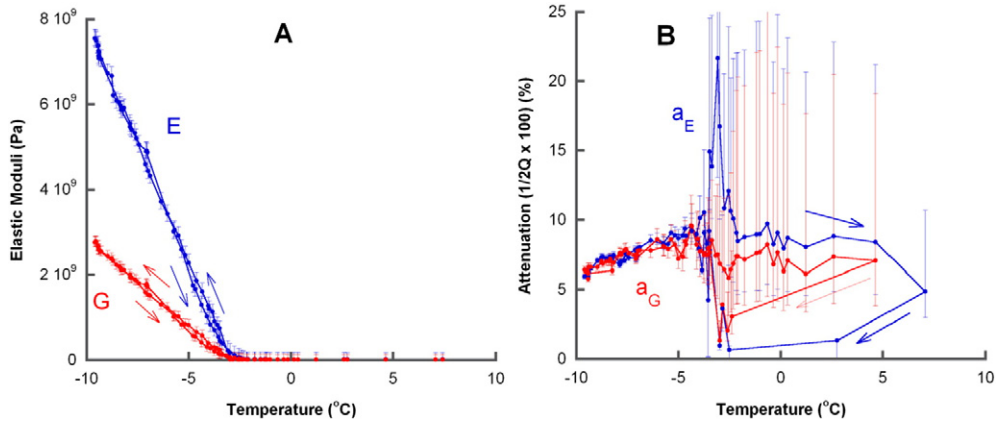


**Fig. 5.** Seismic responses during the experiment. (A) Young's moduli **E** and shear moduli **G** inverted from resonance measurements. The error bars are given for ±10% changes in the jacket stiffness. Below ~−3 °C, both **E** and **G** increase linearly with decreasing temperature. (B) Inverted seismic attenuations. Unlike the moduli, attenuations appear to exhibit a peak immediately below the freezing point, but it is obscured by the large errors above ~−3 °C, the immediate vicinity of the freezing point. The arrows indicate the time history of the experiment following the thaw to freeze sequence. Seismic data was not collected during the initial freezing stage.

measurements on a core sample of the same permafrost to a much lower temperature (~−30 °C) below the eutectic point. If a Poisson's ratio of 0.25 can be assumed, their results indicate that the Young's and Shear modulus would reach ~28 GPa and ~11 GPa, respectively, at a nearly completely frozen state. Thus, the seismic measurements indicate that, at −9 °C, there was still a significant amount of unfrozen water in the sample. This is consistent with the assessment from the electrical resistivity data presented in the previous section. The discussion of unfrozen water content is presented in a later section.

In contrast to the linear increase of stiffness with decreasing temperature, the attenuation appeared to have a peak at temperatures immediately below the freezing point (Fig. 5B). This observation, however, is masked by the large errors in the attenuation data above ~−3 °C. This is because the stiffness of the jacket exceeds the sample stiffness when the soil is unfrozen, making the results of the inversion unreliable. At lower temperatures, both the Young's and shear moduli attenuations decreased gradually (and near linearly for the temperature range of our experiment) in agreement with the results by Spetzler and Anderson (1968) for pure brines, and their behavior was very similar.

### 5.3. Implications for unfrozen water from geophysical data

While both electrical and seismic data indicate the presence of high unfrozen water content in the soil even at the lowest temperature (−9 °C) tested in this experiment, their different behaviors (i.e. differential resistivity signal versus non-differential seismic signal) during the freeze – thaw cycle could help explore the underlying mechanisms controlling the content and distribution of unfrozen water in the soil matrix.

Ice could form in different geometric locations of the pore space and it is generally accepted that ice starts to form in the center of the pore space due to the high chemical potential of its water molecules (Tian et al., 2014). Water molecules bounded to the mineral surface (in the electrical double layer, EDL) or held in small capillaries are more resistive to freezing. The reverse is true during the thawing process, i.e. ice starts to melt from mineral surfaces (Ishizaki et al., 1996). While pore-filling ice formation has the least effects on the soil's elastic properties, ice formed at pore throats has a stronger effect by cementing multiple grains together. Similar effects can be expected for electrical current flow, which are reflected in electrical resistivity measurements.

Two major factors can affect the geophysical and mechanical properties of freezing saline permafrost: unfrozen water content and its spatial distribution. As shown in the models illustrated by Hivon and Sego (1995), while ice occurrence at grain/grain contacts cannot be completely excluded, ice formation in the pore space dominates during freezing of saline soils when the temperature is only moderately low. The relatively small increase of the elastic moduli (Fig. 5A) upon freezing initiation suggests that ice formation likely occurred primarily in the pore space and there was unlikely a significant transition from pore filling to grain cementation mechanism.

Because the seismic measurements are sensitive to the overall effect of these pore scale processes on the bulk soil particularly when low frequencies are used, its non-differential behavior during the freezing and thaw phases suggests the invariability of the mechanical property of the soil at a given temperature regardless of its freeze – thaw history. On the contrary, electrical measurements may have better sensitivity to the local distribution of the electrically conduction pathways, i.e. water films, which may result in differences of electrical resistivity signals depending on whether the soil is undergoing thawing or freezing, as is observed in this experiment. Specifically, the strong shift observed in the electrical resistivity data can result from (Archie, 1942) the difference of the unfrozen water content itself at a given temperature during the freezing versus the thawing phase; (Banin and Anderson, 1974) the difference in the distribution of the unfrozen water and its interconnectedness, in the soil matrix depending on whether the soil is experiencing thawing or freezing; or the combination of both (Archie, 1942) and (Banin and Anderson, 1974). When following the time history of the electrical resistivity data (Fig. 3A), the upward shift of the resistivity curves below the freezing temperatures suggest either a decrease of the unfrozen water content or less connectivity of the water films, or the combination of both, during repeated freezing and thawing processes.

The differential electrical resistivity behavior at the freezing phase present a challenge for unfrozen water content estimation using Archie's law. We demonstrate this using Eq. (5) based on the modified method discussed above. For the soil used in this study, at the room (and reference, $T_0$) temperature (23 °C), ${\sigma^{T0}}_w$ and $\phi^{T0}$ were measured at 6.23 S/m and 0.33, respectively. The cementation exponent $m$ was calculated to have a value of 1.816 at $T_0 = 23$ °C based on bulk and fluid conductivity measured. Eq. (5) shows clearly that the choice of $m$ has a significant impact on the calculated unfrozen water content for a partially frozen soil. For demonstration purpose, we assume $m$ increase to 2.1 at −9 °C following a linear increase with decreasing temperature starting from the freezing point. These $m$ values are within the normal range for saturated soils and rocks. In Fig. 6, we also compare our estimation of unfrozen water content based on resistivity measurements with those presented by Nicolsky and Shakhova, 2010 on a soil with slightly lower salinity (35 ppt) based on the phase diagram presented in Hivon and Sego (1995).

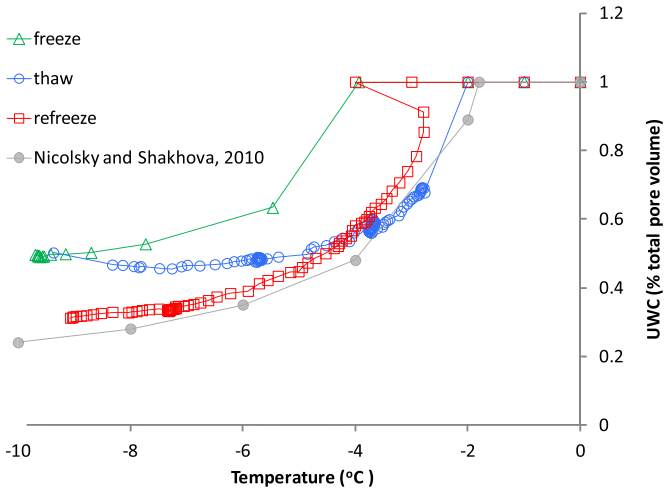


**Fig. 6.** Estimation of the unfrozen water content (UWC) in the saline soil during the initial freeze (green) – thaw (blue) – refreeze (red) cycles based on Archie's law. Variable m values following a linear increase from 1.816 to 2.1 with decreasing temperature from the freezing point to −9 °C were used. Our estimation is compared with the result presented in Nicolsky and Shakhova (2010).

It is apparent from Fig. 6 that large variation in unfrozen water content estimation (ranging from ~30% to ~50% pore volume at ~−9 °C) exists depending on the choice of the resistivity data during the freezing or thawing phase. Among the three different curves, UWC estimation during the refreezing cycle shows the best comparison with data presented by Nicolsky and Shakhova (2010).

While these estimations based on Archie's law show large variability of the unfrozen water content depending on which dataset to use. This discrepancy may be realistic due to the hysteresis effect of the unfrozen water content during freezing versus thawing processes, or it may be due to the uncertainty associated with unfrozen water content estimation based on Archie's law. It is important to note that Archie's law assumes homogeneous media and does not consider the effects of spatial heterogeneity in terms of ice and unfrozen water distribution in the soil matrix.

In saline permafrost, the magnitude of the unfrozen water content hysteresis depends on the impacts of pore fluid salinity on the degree of metastable ice nucleation and the effects on capillary and mineral surface water adsorption (Tian et al., 2014). Supercooling and freezing point depression has been suggested to promote unfrozen water content hysteresis during freeze – thaw cycles (Bittelli and Flury, 2003; Tian et al., 2014). Bittelli and Flury (2003) suggest that during freezing supercooling is responsible for keeping the pore fluid unfrozen below the freezing point until ice nucleation starts, resulting in a larger amount of unfrozen water when compared with the thawing soil at the same temperature. They also suggest that while freezing point depression reduces the ice nucleation temperature to below 0 °C, the ice still melts at 0 °C, generating additional hysteresis in unfrozen water content. While we agree that supercooling can result in hysteresis in unfrozen water content, at least in the temperature range (~−2 to −4 °C) where supercooling occurred, their argument on the discrepancy between the ice nucleation and ice melt temperature is arguable. It is true that ice always nucleate in its pure form, excluding most salts into the remaining liquid water, thus the melting point of this pure ice is always at 0 °C when it is in isolation. However, in water saturated soils, the ice is always in contact with the mineral grains or high salinity unfrozen water (very high salinity in our case). This causes the ice to start melting at temperatures below 0 °C, particularly in high salinity or high clay content soils. This is similar to the freezing point depression effect, but only in the reversed process (i.e. thawing instead of freezing).

In addition to supercooling and freezing point depression, the presence of salt in pore water can affect unfrozen water hysteresis through its impact on the EDL properties and surface tension, thus associated capillary and surface water adsorption effects. The Guoy - Chapman model (Stumm and Morgan, 1996) predicts a decrease of the EDL thickness proportional to the square root of salt concentration. Therefore, the presence of salt in the pore water compresses the EDL, leading to a less significant capillary and surface adsorption effects, thus a potentially smaller hysteresis effect. In our study, combining the supercooling, freezing point depression and the surface effects will likely result in some degree of hysteresis during the freeze – thaw cycles, particularly in the temperature range where supercooling occurred. However, this effect is difficult to quantify.

The non-differential seismic data during the freezing versus thawing phase likely suggest that the unfrozen water hysteresis effect may not be significant enough to result in observable changes in the elastic properties in the range of the temperature tested. Therefore, it is likely that hysteresis only partially contribute to the large variation of the unfrozen water content estimation shown in Fig. 4 based on Archie's law, and that this large variation could partially due to the limitation of the Archie's law in terms of its use for unfrozen water content estimation in partially frozen soil. We could relate this to the heterogeneous distribution of the ice and unfrozen water in the permafrost soil, its dynamic change during different freezing or thawing cycles and the subsequent impact on the choice of the cementation exponent *m* when applying Archie's law. The upward shift of the resistivity data shown in Fig. 4 is likely due to the change of the distribution pattern of the ice or unfrozen water in the soil matrix during repeated freeze – thaw cycles with some moderate hysteresis effects. Further investigations involving independent validation of the unfrozen water content and interfacial scale modeling of ice nucleation and growth are needed to confirm these proposed mechanisms.

## 6. Conclusions

We conducted laboratory studies on the geophysical signals from saline permafrost soils and how they can help to understand the physical and mechanical process during freeze-thaw cycles. Both the electrical and seismic measurements revealed the physical and mechanical properties of the saline permafrost soils within the similar temperature range encountered in the shallow subsurface near barrow, AK. Temperature induced freeze – thaw transition of the permafrost soil was characterized by significant change of the electrical and seismic signals in terms of the magnitude of the signal and the rate of change. While electrical resistivity signal captured the transient supercooling behavior of the soil during the freezing phase, the induced polarization measurements demonstrated a systematic shift of the SIP spectrum to smaller magnitude and lower frequency during the freezing process that were likely caused by increase of salinity of the unfrozen water, decrease of temperature as well as ice formation. A characteristic IP anomaly at 1 Hz during the onset of freezing (i.e. ice formation) was first observed in our experiment although its underlying mechanism is unclear.

Sonic-frequency seismic measurements revealed linear changes in the Young's and shear moduli (i.e., the mechanical strength) of the soil, which were substantially smaller than completely frozen soils at the lowest temperature tested (~−10 °C). This, together with the observation of reduced but still large attenuations at $Q_E$ and $Q_G$ at this temperature, confirms the presence of a significant amount of unfrozen water, consistent with indication from the electrical measurements where the electrical resistivity is still very low at −9 °C.

Our results demonstrated the uncertainty of using Archie's law to estimate the unfrozen water content in saline permafrost based on electrical resistivity measurements. Specifically, the choice of the cementation exponent and the specific resistivity during either a freezing or thawing phase can have a major effects on the estimated unfrozen

water content. Joint interpretation of the electrical and seismic data suggest that rather than a realistic and significant difference in the unfrozen water content, the differential electrical signal observed during the experiment may be related to the change of the distribution pattern of ice and unfrozen water between the freezing and the thawing cycle of the soil. Collectively, our results provide an improved petrophysical understanding of the physical and mechanical properties of saline permafrost during freeze – thaw transitions, and suggest that cautions need to be exercised when interpreting geophysical data collected at field scales in terms of its use for unfrozen water content estimation.

## Acknowledgement

The Next-Generation Ecosystem Experiments (NGEE Arctic) project is supported by the Office of Biological and Environmental Research in the DOE Office of Science. We acknowledge Craig Ulrich (LBNL), John Peterson (LBNL), Alexander Kholodov (UAF), Cathy Wilson (LANL) and David Graham (ORNL) for their help with field coring efforts. This NGEE-Arctic research is supported through contract number DE-AC0205CH11231 to Lawrence Berkeley National Laboratory. We gratefully acknowledge the project PI, Stan Wullschleger at ORNL. The datasets presented in this research are available at http://dx.doi.org/10.5440/1374172.

## References

Archie, G.E., 1942. The electrical resistivity log as an aid in determining some reservoir characteristics: transactions of the American Institute of Mineral. Metallurgy and Petroleum Engineers 146, 54–62.
Banin, A., Anderson, D.M., 1974. Effects of salt concentration changes during freezing on the unfrozen water content of porous materials. Water Resour. Res. 10 (1), 124–128.
Banville, D.R., Fortier, R., Dupuis, C., 2016. Objective interpretation of induced polarization tomography using a quantiative approach for the investigation of periglacial environments. J. Appl. Geophys. 130, 218–233.
Bittelli, M., Flury, M., 2003. A thermodielectric analyzer to measure the freezing and moisture characteristic of porous media. Water Resour. Res. 39 (2), 1041.
Bjerrum, N., 1952. Structure and properties of ice. Science 115, 385–390.
Brouchkov, A., 2003. Frozen Saline Soils of the Arctic Coast: Their Distribution and Engineering Properties: Proceedings of the 8th International Conference on Permafrost. 95–100. National Academy of Sciences.
Carcione, J.M., Gei, D., 2004. Gas-hydrate concentration estimated from P- and S-wave velocities at the Malik 2L-38 research well, Mackenzie Delta, Canada. Journal of Applied Geophysics 56, 73–78.
Carcione, J.M., Campanella, O.O., Santos, J.E., 2007. A poroelastic model for wave propagation in partially frozen orange jouice. J. Food Eng. 80, 11–17.
Dafflon, B., Hubbard, S., Ulrich, C., Peterson, J., 2013. Electrical conductivity imaging of active layer and permafrost in an Arctic ecosystem, through advanced inversion of electromagnetic induction data. Vadose Zone J. 12 (4).
Dafflon, B., Hubbard, S.S., Ulrich, C., Peterson, J.E., Wu, Y., Wainwright, H., Kneafsey, T., 2016. Geophysical estimation of shallow permafrost distribution and properties in an ice-wedge polygon-dominated Arctic tundra region. Geophysics 81 (1), WA247–WA263.
Daniels, J.J., Keller, G.V., Jacobson, J.J., 1976. Computer-assisted interpretation of electromagnetic soundings over a permafrost section. Geophysics 41 (4), 752–765.
Dou, S., Ajo-Franklin, J.B., 2014. Full wavefield inversion of surface waves for mapping embedded low-velocity zones in permafrost. Geophysics 79 (6), EN107–EN124.
Dou, S., Nakagawa, S., Dreger, D., Ajo-Franklin, J.B., 2016. A rock-physics investigation of unconsolidated saline permafrost: P-wave properties from laboratory ultrasonic measurements. Geophysics 81 (1), WA233–WA245.
Dou, S., Nakagawa, S., Dreger, D., Ajo-Franklin, J.B., 2017. An effective-medium model for P-wave velocities of saturated, unconsolidated saline permafrost. Geophysics 82 (3), EN33–EN50.
Fortier, R., Allard, M., 1998. Induced polarization and resistivity logging in parmafrost. Proceedings at Seventh International Permafrost Conference, at Yellowknife (Canada).
Fortier, R., LeBlanc, A.-M., Allard, M., Buteau, S., Calmels, F., 2008. Internal structure and conditions of permafrost mounds at Umiujaq in Nunavik, Canada, inferred from field investigation and electrical resistivity tomography. Canadian Journal of Earth Sciences/Revue Canadienne des Sciences de la Terre 45, 367–387.
French, H.K., Binley, A., Kharkhordin, I., Kulessa, B., Krylov, S., 2006. Cold regions hydrogeophysics: physical characterisation and monitoring. In: Vereecken, H., et al. (Eds.), Applied Hydrogeophysics. 195–232. Springer.
Frolov, A.D., 1973. Elastic and electrical properties of frozen ground. Proceedings at 2nd International Conference on Permafrost.
Glover, P., 2009. What is the Cementation Exponent? A New Interpretation. The Leading Edge. 82–85.
Grimm, R.E., Stillman, D.E., Dec, S.F., Bullock, M.A., 2008. Low-frequency electrical properties of polycrystalline saline ice and salt hydrates. J. Phys. Chem. B 112, 15382–15390.
Hauck, C., 2012. Frozen ground monitoring using DC resistivity tomography. Geophys. Res. Lett. 29 (21):2016. http://dx.doi.org/10.1029/2002GL014995.
Hayley, K., Bentley, L.R., Gharibi, M., Nightingale, M., 2007. Low temperature dependence of electrical resistivity: implications for near surface geophysical monitoring. Geophys. Res. Lett. 34, L18402 doi:18410.11029/12007GL031124.
Hilbich, C., Hauck, C., Hoelzle, M., Scherler, M., Schudel, L., Volksch, I., Muhll, D.V., Mausbacher, R., 2008. Monitoring mountain permafrost evolution using electrical resistivity tomography: a 7-year study of seasonal, annual, and long-term variations at Schilthorn, Swiss Alps. J. Geophys. Res. 113:F01S90. http://dx.doi.org/10.1029/2007JF000799.
Hivon, E.G., Sego, D.C., 1993. Distribution of saline permafrost in the Northwest territories, Canada. Can. Geotech. J. 30, 506–514.
Hivon, E.G., Sego, D.C., 1995. Strength of frozen saline soils. Can. Geotech. J. 32, 336–354.
Hubbard, S., Gangodagamage, C., Dafflon, B., Wainwrite, H., Peterson, J., Gusmeroli, A., Ulrich, C., Wu, Y., Wilson, C., Rowland, J., Tweedie, C.T., Wullschleger, S.D., 2013. Quantifying and relating subsurface and land-surface variability in permafrost environments using surface geophysical and Lidar datasets. Hydrogeol. J. 21 (1), 149–169.
Humlum, O., Instanes, A., Sollid, J.L., 2003. Permafrost in Svalbard: a review of research history, climatic background and engineering challenges. Polar Res. 22 (2), 191–215.
Ishizaki, T., Maruyama, M., Furkawa, Y., Dash, J.G., 1996. Premelting of ice in porous silica glass. J. Cryst. Growth 163, 455–460.
Jahnert, S., Chavez, F.V., Schaumann, G.E., Schreiber, A., Schonhoff, M., Findenegg, G.H., 2008. Melting and freezing of water in cylindrical silica nanopores. Phys. Chem. Chem. Phys. 10, 6039–6051.
King, M.S., Zimmerman, R., Corwin, R.F., 1988. Seismic and electrical properties of unconsolidated permafrost. Geophys. Prospect. 36, 349–364.
Kneafsey, T.J., Lu, H., Boswell, R., Hunter, R., Collett, T.S., 2011. Examination of core samples from the Mount Elbert gas hydrate stratigraphic test well, Alaska North Slope: effects of retrieval and preservation. Mar. Pet. Geol. 28 (2), 381–393.
Krautblatter, M., Hauck, C., 2007. Electrical resistivity tomography monitoring of permafrost in solid rock walls. J. Geophys. Res. 112:F02S20. http://dx.doi.org/10.1029/2006JF000546.
Krautblatter, M., Zisser, N., 2012. Laboratory evidence for linear temperature-resistivity pathways of thawed, supercooled and frozen permafrost rocks. Geophys. Res. Lett. (In press).
Krautblatter, M., Verleysdonk, S., Flores-Orozco, A., Kemna, A., 2010. Temperature-calibrated imaging of seasonal changes in permafrost rock walls by quantitative electrical resistivity tomography (Zugspitze, German/Austrian Alps). J. Geophys. Res. 115, F02003 doi:02010.01029/02008JF001209.
Kruschwitz, D.S.F., 2008. Assessment of the Complex Resistivity Behavior of Salt Affected Building Materials. Technical University of Berlin.
Krylov, S., Bobrov, N.Y., 1998. Anomalous electrical properties of saline permafrost on the Yamal Peninsula, Northwestern Siberia, from field electromagnetic survey. Proceedings at Seventh International Conderence on Permafrost, at Yellowknife, Canada.
Kurfurst, P.J., 1976. Ultrasonic wave measurements on frozen soils at permafrost temperatures. Can. Geotech. J. 13, 1571–1576.
Kuster, G.T., Toksoz, M.N., 1974. Velocity and attenuation of seismic waves in two phase media: part I. Theorectical formulations. Geophysics 39, 587–606.
Lee, S., Pyrak-Nolte, L.J., Cornillon, P., Campanella, O., 2004. Characterization of frozen orange juice by ultrasound and wavelet analysis. J. Sci. Food Agric. 84, 405–410.
Lesmes, D.P., Frye, K.M., 2001. The influence of pore fluid chemistry on the complex conductivity and induced-polarization responses of Berea Sandstone. J. Geophys. Res. 106, 4079–4090.
Maeno, N., Araki, T., Moore, J., Fukuda, M., 1992. Dielectric response of water and ice in frozen soils. In: Maeno, N., Hondoh, T. (Eds.), Physics and Chemistry of Ice. Hokkaido University Press.
Marion, G.M., 1995. Freeze-thaw processes and soil chemistry. Cold Regions Research & Engineering Laboratory, Special Report 95-12.
Matsushima, J., Suzuki, M., Kato, Y., Nibe, T., Rokugawa, S., 2008. Laboratory experiments on compressional ultrasonic wave attenuation in partially frozen brines. Geophysics 73, N9–18.
Minsley, B.J., Abraham, J.D., Smith, B.D., Cannia, C., Voss, C.I., Jorgenson, M.T., Walvoord, M.A., Wylie, B.K., Anderson, L., Ball, L.B., Deszcz-Pan, M., Wellman, T.P., Ager, T.A., 2012. Airborne electromagnetic imaging of discontinuous permafrost. Geophys. Res. Lett. 39, L02503.
Nakagawa, S., 2011. Split Hopkinson resonant bar test for sonic-frequency acoustic velocity and attenuation measurements of small, isotropic geological samples. Rev. Sci. Instrum. 82, 044901.
Nicolsky, D., Shakhova, N., 2010. Modeling sub-sea permafrost in the East Siberian Arctic Shelf: the Dmitry Laptev Strait. Environ. Res. Lett. 5, 015006.
Nixon, J.F., 1987. Pile load tests in saline permafrost at Clyde River, Northwest Territories. Can. Geotech. J. 25, 24–32.
Oldenborger, G., LeBlanc, A., 2015. Geophysical characterization of permafrost terrain at Iqaluit International Airport, Nunavut. J. Appl. Geophys. 123, 36–49.
Olhoeft, G.R., 1977. Electrical properties of natural clay permafrost. Canadian Journal of Earth Sciences/Revue Canadienne des Sciences de la Terre 14, 16–24.
Osterkamp, T.E., 2001. Subsea permafrost. In: Steele, J.H., Thorpe, S.A., Turekian, K.K. (Eds.), Encyclopedia of Ocean Sciences. Academic Press, pp. 2902–2912.
Patterson, D.E., Smith, M.W., 1984. Unfrozen water content in saline soils: results using time-domain reflectometry. Can. Geotech. J. 22, 95–101.
Petrenko, V.F., Whitworth, R.W., 1999. Physics of Ice. Oxford University Press.
Potter, R.W., Clynne, M.A., Brown, D.L., 1978. Freezing-point depression of aqueous sodium-chloride solutions. Econ. Geol. 73 (2), 284–285.

Scherler, M., Hauck, C., Hoelzle, M., Stahli, M., Volksch, I., 2011. Meltwater infiltration into the frozen active layer at an alpine permafrost site. Permafr. Periglac. Process. 21 (4), 325–334.
Slater, L., Choi, J., Wu, Y., 2005. Electrical properties of iron-sand columns: implications for induced polarization investigation and performance monitoring of iron-wall barriers. Geophysics 70 (4).
Smith, M.W., Tice, A.R., 1988. Measurement of the Unfrozen Water Content of Soils — Comparison of NMR and TDR Methods. Cold Regions Research & Engineering Laboratory.
Spetzler, H., Anderson, D.L., 1968. The effect of temperature and partial melting on velocity and attenuation in a simple binary system. J. Geophys. Res. 73, 6051–6060.
Stillman, D.E., Grimm, R.E., S. F., Dec. 2010. Low-frequency electrical properties of ice-silicate mixtures. J. Phys. Chem. B 114, 6065–6073.
Stumm, W., Morgan, J.J., 1996. Aquatic Chemistry: Chemical Equlibria and Rates in Natural Waters. John Wiley & Sons, Inc.
Tian, H., Wei, C., Wei, H., Zhou, J., 2014. Freezing and thawing characteristics of frozen soils: bound water content and hysteresis phenomenon. Cold Reg. Sci. Technol. 103, 74–81.
Tong, M., Tao, H., 2007. Experimental study of induced polarization relaxation time spectra of shaly sands. J. Pet. Sci. Eng. 59, 239–249.
Velli, Y.Y., Grishin, P.A., 1982. On the functional dependence of the freezing point of soils on the composition of water soluble salts in an interstitial solution (translated from Russian). Rheology of Soils and Engineering Geocryology 193–196.
Vinegar, H.J., Waxman, M.H., 1984. Induced polarization of shaly sands. Geophysics 49, 1267–1287.
Watanabe, K., Mizoguchi, M., 2002. Amount of unfrozen water in frozen porous media saturated with solution. Cold Reg. Sci. Technol. 34, 103–110.
Winer, K.W., Nur, A., 1979. Pore fluid and seismic attenuation in rock. Geophys. Res. Lett. 6, 1–4.
Worthington, P.F., Collar, F.A., 1984. Relevance of induced polarization to quantitative formation evaluation. Mar. Pet. Geol. 1 (1), 14–26.
Wu, Y., Hubbard, S., Ulrich, C., Wullschleger, S.D., 2013. Remote monitoring of freeze-thaw transitions in arctic soils using the complex resistivity method. Vadose Zone J. 12 (1).
Wu, Yuxin, Nakagawa, Seiji, Kneafsey, Timothy J., 2017. Electrical and Seismic Response of Saline Permafrost Soil during Freeze - Thaw Transition: Supporting Data. Next Generation Ecosystem Experiments Arctic Data Collection, Carbon Dioxide Information Analysis Center, Oak Ridge National Laboratory, Oak Ridge, Tennessee, USA Data accessed at. http://dx.doi.org/10.5440/1374172.
Zisser, N., Kemna, A., Nover, G., 2010. Dependence of spectral-induced polarization response of sandstone on temperature and its relevance to permeability estimation. J. Geophys. Res. 115, B09214 doi: 09210.01029/02010JB007526.